

AD-A234 191

2

NAVAL POSTGRADUATE SCHOOL Monterey, California



THESIS

COMPARISON OF SOUND PRESSURE IN A
WEDGE-SHAPED OCEAN AS
PREDICTED BY AN IMAGE METHOD AND A PE
MODEL

by

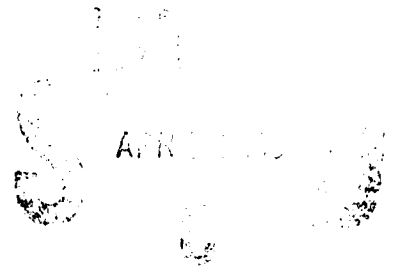
Kim, Jong Rok

December 1990

Co-Advisor
Co-Advisor

Alan B. Coppens
James V. Sanders

Approved for public release; distribution is unlimited.



91 4 01 005

Unclassified

security classification of this page

REPORT DOCUMENTATION PAGE				
1a Report Security Classification Unclassified		1b Restrictive Markings		
2a Security Classification Authority		3 Distribution/Availability of Report Approved for public release; distribution is unlimited.		
2b Declassification Downgrading Schedule		5 Monitoring Organization Report Number(s)		
4 Performing Organization Report Number(s)				
6a Name of Performing Organization Naval Postgraduate School		6b Office Symbol (if applicable) PII	7a Name of Monitoring Organization Naval Postgraduate School	
6c Address (city, state, and ZIP code) Monterey, CA 93943-5000		7b Address (city, state, and ZIP code) Monterey, CA 93943-5000		
8a Name of Funding/Sponsoring Organization		8b Office Symbol (if applicable)	9 Procurement Instrument Identification Number	
8c Address (city, state, and ZIP code)		10 Source of Funding Numbers		
		Program Element No	Project No	Task No
		Work Unit Accession No		
11 Title (Include security classification) COMPARISON OF SOUND PRESSURE IN A WEDGE-SHAPED OCEAN AS PREDICTED BY AN IMAGE METHOD AND A PE MODEL.				
12 Personal Author(s) Kim, Jong Rok				
13a Type of Report Master's Thesis		13b Time Covered From To	14 Date of Report (year, month, day) December 1990	15 Page Count 46
16 Supplementary Notation The views expressed in this thesis are those of the author and do not reflect the official policy or position of the Department of Defense or the U.S. Government.				
17 Cosati Codes			18 Subject Terms (continue on reverse if necessary and identify by block number)	
Field	Group	Subgroup	Image Method, Parabolic Equation Model, Wedge-shaped Ocean	
19 Abstract (continue on reverse if necessary and identify by block number) Predictions of the sound pressure field in a wedge-shaped ocean overlying a fast bottom have been generated by computer-implemented calculations based on a method of images model and two parabolic equation models. Comparisons of the results show significant agreements and also some disagreements. The geometric shape of the wedge for the image calculation consists of a plane, sloping penetrable bottom and a plane, horizontal pressure release upper surface. This shape models a real continental shelf. The shape used in the parabolic equation models is a pressure release plane surface above a conical bottom. Two PE models were studied. One, from a literature, is based on a wide-angle parabolic equation and providing a contour plot of TL as a function of position. The other, resident on the NPS computer, is based on an implicit finite-difference (IFD) algorithm. The results show that there is fair agreement among the different models. Comparison of the image method and the second PE model shows a 2 to 3 dB difference in transmission loss near the surface and good agreement deeper. The transmission loss predicted by the first PE model differs from both other models by 4 to 5 dB near the surface and at the middle depths. Near the bottom they all agree well.				
20 Distribution/Availability of Abstract <input checked="" type="checkbox"/> unclassified-unlimited <input type="checkbox"/> same as report <input type="checkbox"/> DTIC users			21 Abstract Security Classification Unclassified	
22a Name of Responsible Individual Alan B. Coppens			22b Telephone (Include Area code) (408) 646-2116	22c Office symbol PII/Sd

DD FORM 1473,84 MAR

83 APR edition may be used until exhausted
All other editions are obsolete

security classification of this page

Unclassified

**BEST
AVAILABLE COPY**

Approved for public release; distribution is unlimited.

Comparison of Sound Pressure in a Wedge-shaped Ocean as
Predicted by an Image Method and a PE Model

by

Kim, Jong Rok
Lt., Korean Navy
B.S., Korean Naval Academy, 1983

Submitted in partial fulfillment of the
requirements for the degree of

MASTER OF SCIENCE IN ENGINEERING ACOUSTICS

from the

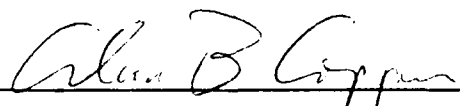
NAVAL POSTGRADUATE SCHOOL
December 1990

Author:



Kim, Jong Rok

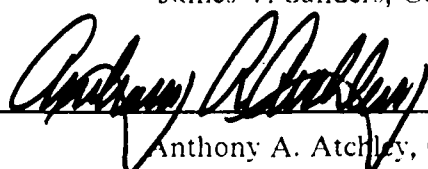
Approved by:



Alan B. Coppens, Co-Advisor



James V. Sanders, Co-Advisor



Anthony A. Atchley, Chairman,
Engineering Acoustics Academic Committee

ABSTRACT

Predictions of the sound pressure field in a wedge-shaped ocean overlying a fast bottom have been generated by computer-implemented calculations based on a method of images model and two parabolic equation models. Comparisons of the results show significant agreements and also some disagreements. The geometric shape of the wedge for the image calculation consists of a plane, sloping penetrable bottom and a plane, horizontal pressure release upper surface. This shape models a real continental shelf. The shape used in the parabolic equation models is a pressure release plane surface above a conical bottom. Two PE models were studied. One, from a literature, is based on a wide-angle parabolic equation and providing a contour plot of TL as a function of position. The other, resident on the NPS computer, is based on an implicit finite-difference (IFD) algorithm. The results show that there is fair agreement among the different models. Comparison of the image method and the second PE model shows a 2 to 3 dB difference in transmission loss near the surface and good agreement deeper. The transmission loss predicted by the first PE model differs from both other models by 4 to 5 dB near the surface and at the middle depths. Near the bottom they all agree well.

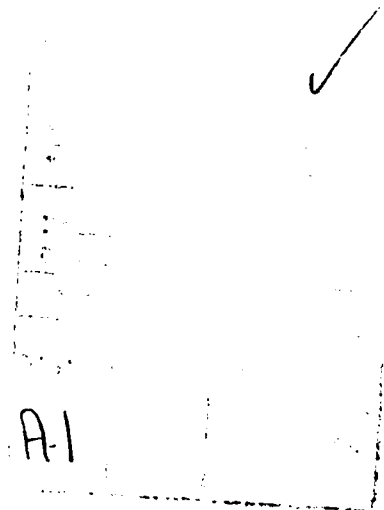


TABLE OF CONTENTS

I. INTRODUCTION.....	1
II. DEVELOPMENT	3
A. IMAGE THEORY	3
B. PE MODEL	12
III. COMPUTATION OF IMAGE METHOD	13
IV. DISCUSSION.....	19
A. IMAGE METHOD AND PESAC	19
B. IMAGE METHOD AND PEIFD	24
V. CONCLUSIONS.....	34
APPENDIX.....	35
LIST OF REFERENCES.....	37
INITIAL DISTRIBUTION LIST.....	38

ACKNOWLEDGEMENT

I wish to thank Professors James V. Sanders and Alan B. Coppens for their kind instruction, support and perseverance in this work.

I INTRODUCTION

Acoustic propagation in an ocean with a sloping bottom is of growing concern both for theoretical reasons and because of the importance of knowing the performance of acoustic sensors located over the continental slope. This problem has been studied by many scientists. In this research we compare and contrast the results of three different models, predicting the pressure field in a wedge-shaped ocean with a pressure release surface and an acoustically fast bottom. One image method and two PE models were selected.

The computer model for the image method was written in Basic for use on a PC and in Fortran for use on the NPS IBM 3033 computer main frame. The majority of the computations for the image method was done using the Fortran version.

A PE model contained in "Ocean Exec" library on the NPS IBM 3033 computer was tested, but found to be too cumbersome and time-consuming. Modeling a sloping bottom with acceptable accuracy required 100 pairs of range-depth input which is tedious. In addition the program needs knowledge of certain parameters for a basement layer which is required to exist below the bottom. The output gives transmission loss at a fixed depth. To find the TL as a function of range for various depths between the bottom and the surface necessitated running the program many times which would have required an unacceptable amount of computer time. For these reasons, this PE model was not used for this work.

Two other PE models were found to be more acceptable. One was a model used at SACLANT by Tindle and Jensen [Ref. 1] which we will refer to as PESAC. The other was a model based on an implicit finite-difference (IFD) algorithm implemented at NPS by Jaeger [Ref. 2]; we refer to this model as PEIFD in what follows. PESAC was not available for use, but some of its output was in the referenced article in the form of a contour plot of TL vs position in and below the wedge for a stated set of water and bottom parameters. The PEIFD, being available at NPS, was used to generate output for the same set of parameters. The results of the image method model and the two PE models are compared in the analysis that follows.

II. DEVELOPMENT

A. IMAGE THEORY

In 1978, with the aid of a computer model based on the method of images, Coppens, Sanders, Ioannou, and Kawamura [Ref. 3] predicted and measured the pressure amplitude and phase in the upslope direction along the bottom of a wedge-shaped fluid layer overlying a fast fluid bottom. Baek [Ref. 4] used the same model in 1984 to predict pressure amplitude and phase everywhere within the wedge in the upslope direction. In the same year, LeSesne [Ref. 5] implemented a model developed by Coppens and Sanders which is not limited to up or downslope direction. In the method of images, boundaries are replaced by images of the source, placed geometrically to represent the propagation path between source and field point and given amplitudes and phases to reproduce the effects of interactions with the boundaries. For a wedge-shaped duct, images lie on a circle centered at the apex of the wedge. The source and each of the images radiate spherical waves of appropriate phases and amplitudes. The phase coherent summation of these waves yields the total pressure and phase at any field point in the wedge. In the computer program the number of images is made finite by insisting that the wedge angle β is an integral submultiple of 180° . Then, the number of images (including the source) in upper or lower half-spaces is

$$N = (180/\beta) \tag{1}$$

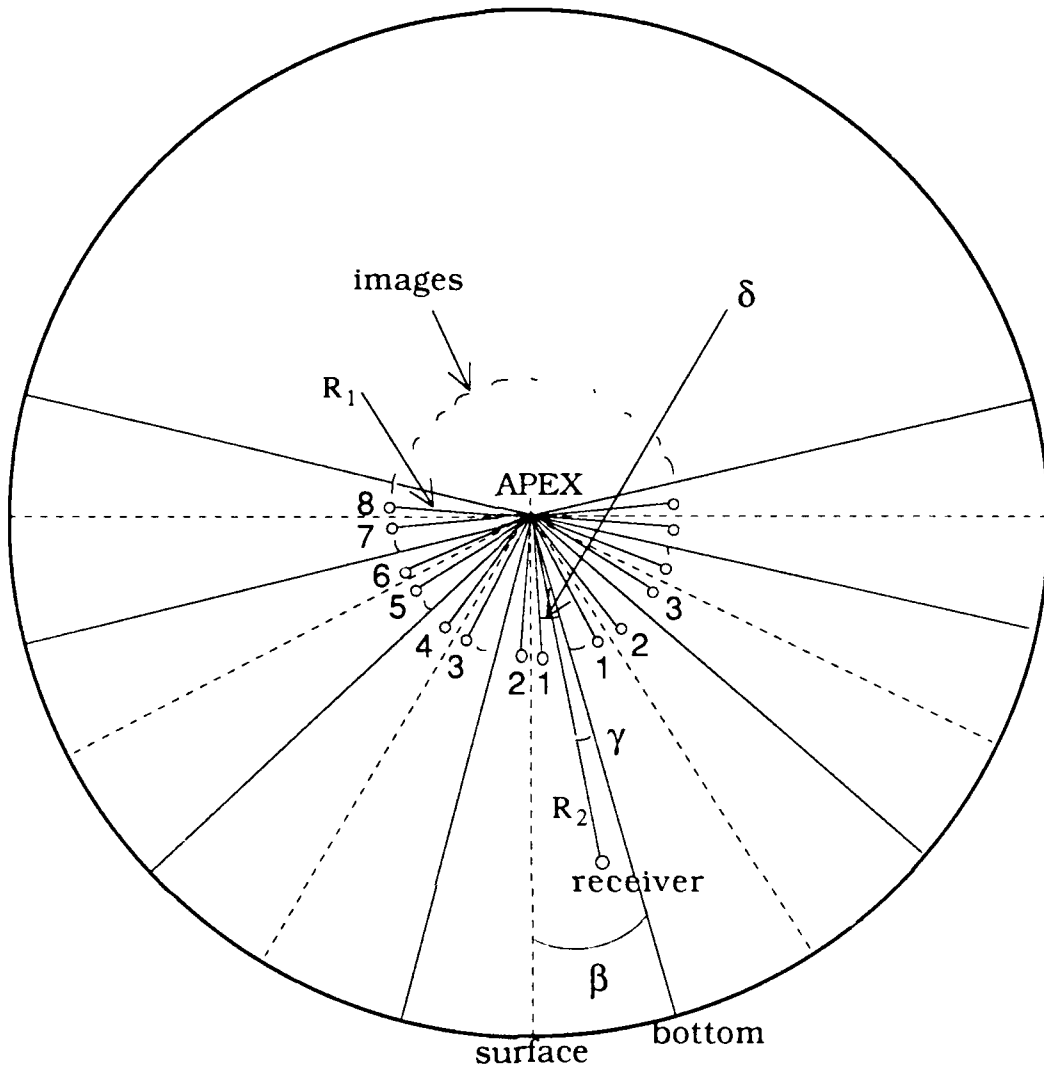
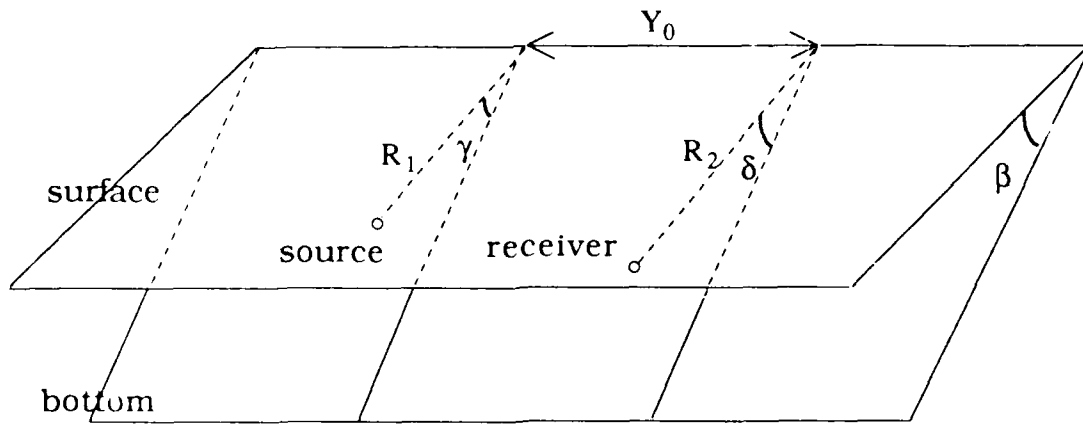


Figure 1. Image structure for a wedge shaped duct (side view)

The geometry of the image method is represented in Fig. 1. Figure 2 contains the definitions and symbols for source and receiver parameters.



- β = wedge angle
 R_1 = scaled distance from apex to the source
 R_2 = scaled distance from apex to the receiver
 Y_0 = scaled distance along the shore between the receiver and the source
 γ = source angle measured upward from the interface
 δ = receiver angle measured upward from the interface
 D_1 = the ratio of medium density to the bottom density
 CC = the ratio of medium (water) sound speed to the bottom sound speed
 θ_c = critical angle for the bottom
 X = scaling distance
 α/k_2 = loss term in the bottom (used in the reflection coefficient)
 $R(n)$ = range from the nth image to the receiver

Figure 2. Definitions and notations of source and receiver parameters

For the wedge-shaped duct, sound will propagate from the source to the receiver through paths that can be divided into two families: (1) direct, surface reflected, surface then bottom reflected, surface-bottom-surface, and so on; (2) bottom reflected, bottom-surface reflected, bottom-surface-bottom, and so on. For example, the bottom-surface-bottom path to the receiver in Fig. 3(a) can be interpreted as the straight line connecting the 3rd image with the receiver in Fig. 3(b).

The angle θ_n of the n^{th} image measured from the bottom is shown in Fig. 1,

$$\theta_n = \beta(n-1) + \gamma, \quad \text{for } n \text{ odd} \quad (2.1)$$

$$\theta_n = \beta n - \gamma, \quad \text{for } n \text{ even} \quad (2.2)$$

The pressure from an image can be determined knowing the distance between the image and the receiver and the total reflection coefficient. The total reflection coefficient is the product of all reflection coefficients along the path from image to receiver. With pressure one meter from the source normalized to unity, the pressure at a field point from a specific image is found by dividing this total reflection coefficient by the distance.

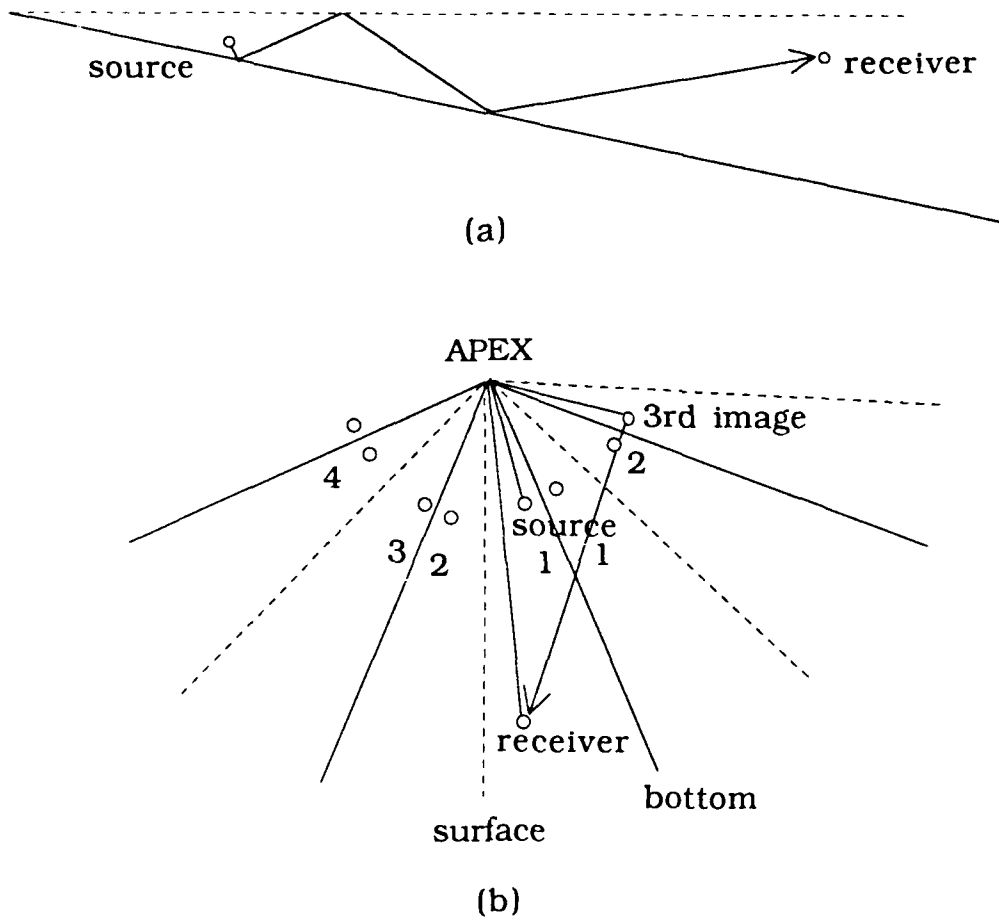


Figure 3. Visualization of (a) real path and (b) equivalent path in image method

The distance between the receiver and the n^{th} image, as shown in Fig. 4 is

$$R(n) = \sqrt{R_1^2 + R_2^2 - 2R_1R_2 \cos(\theta_n - \delta) + Y_0^2} \quad (3.1)$$

for the upper group of images, and

$$R'(n) = \sqrt{R_1^2 + R_2^2 - 2R_1R_2 \cos(\theta_n + \delta) + Y_0^2} \quad (3.2)$$

for the lower group of images.

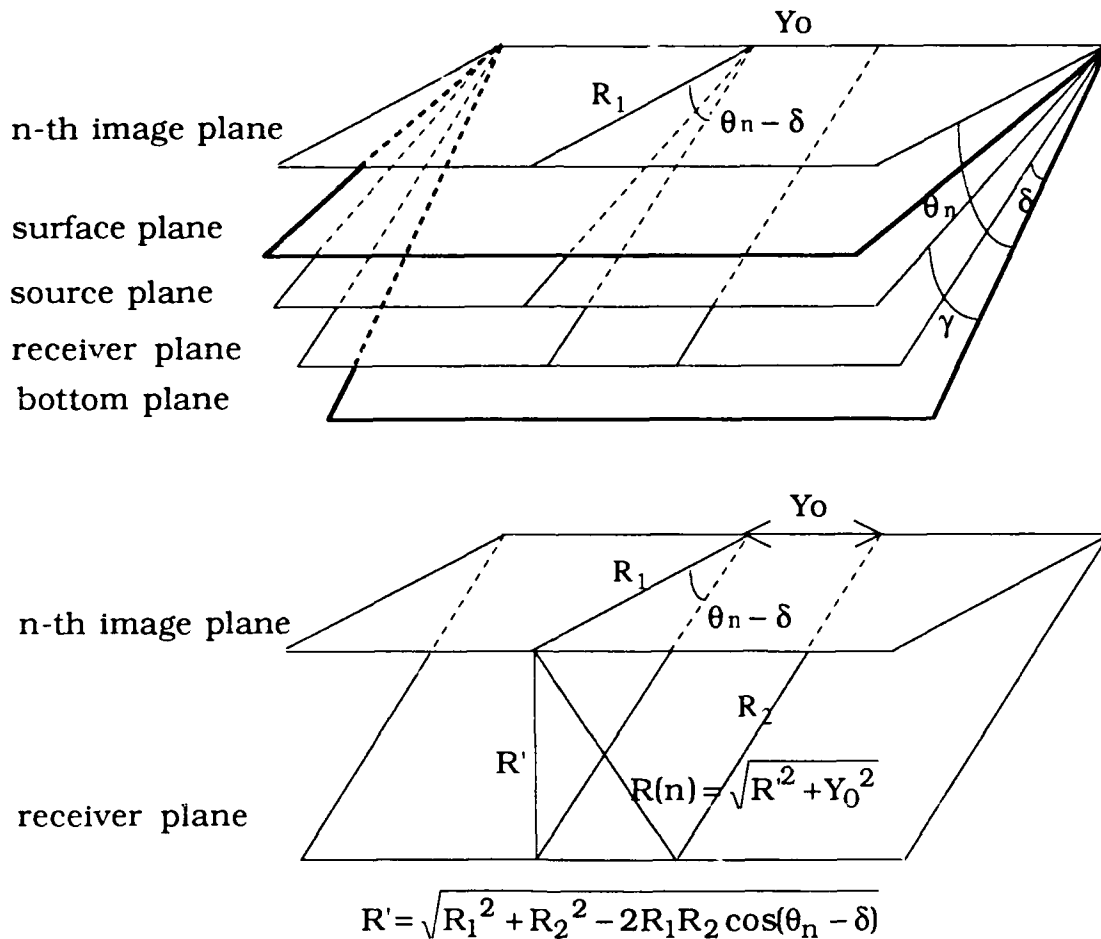
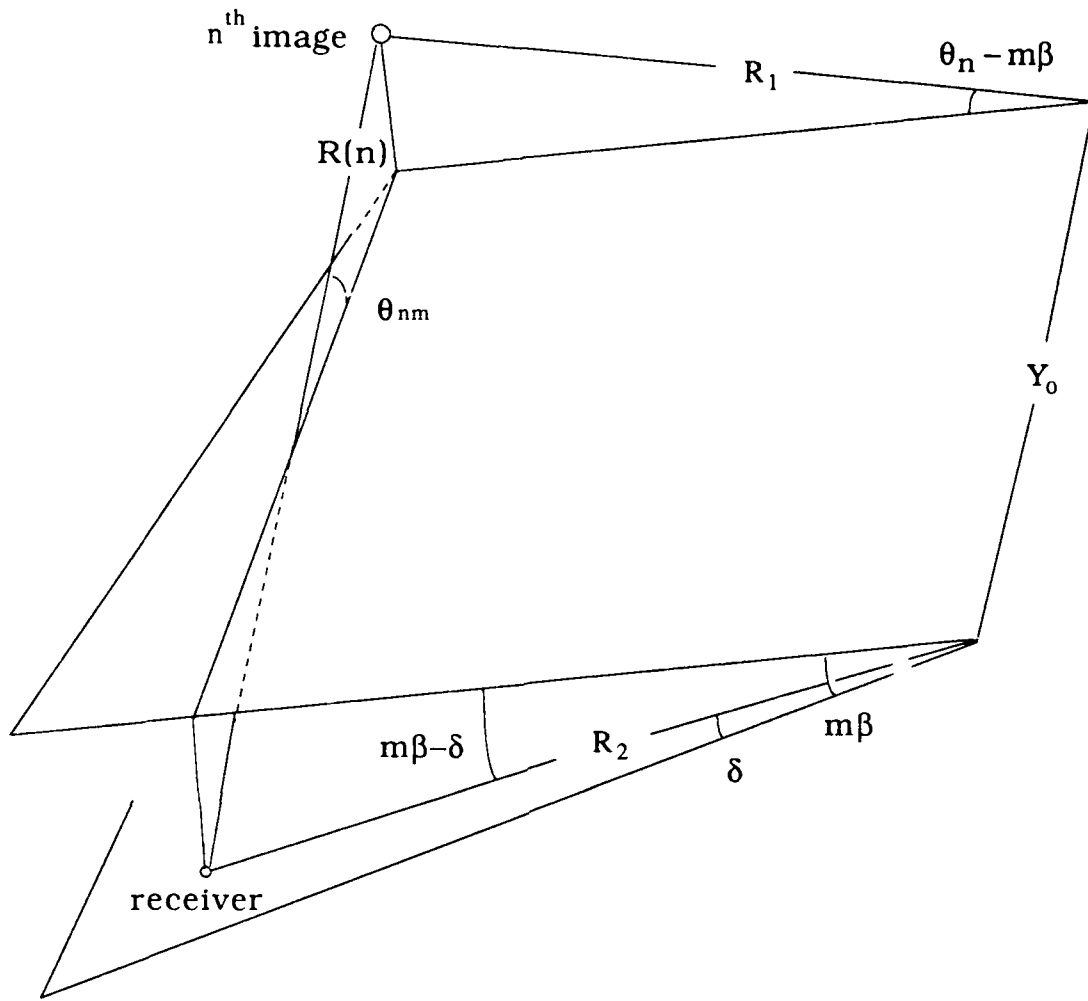


Figure 4. The distance $R(n)$ between receiver and n^{th} image

From Fig. 2, each image interacts with the bottom and surface a number of times: so that the pressure at the receiver from a specific image is proportional to the product of the relevant reflection coefficients. To find a reflection coefficient, the angle of incidence must be determined. The greater the index n of the image, the more reflections, and one must find an incident angle for each of these reflections.



$$\sin(\theta_{nm}) = \frac{R_1 \sin(\theta_n - m\beta) + R_2 \sin(m\beta - \delta)}{R(n)}$$

Figure 5. The angle of incidence θ_{nm} of the upper n^{th} image on the m^{th} plane

The angle of incidence on the m^{th} plane for the n^{th} image θ_{nm} is given by (Fig. 5):

$$\sin(\theta_{nm}) = \frac{R_1 \sin(\theta_n - 2m\beta) + R_2 \sin(2m\beta - \delta)}{R(n)}, \quad m = 1, 2, 3, \dots \quad (4.1)$$

for the upper images,

$$\sin(\theta'_{nm}) = \frac{R_1 \sin(\theta'_n - 2m\beta) + R_2 \sin(2m\beta + \delta)}{R'(n)}, \quad m = 0, 1, 2, 3, \dots \quad (4.2)$$

for the lower images. [The notation is θ for the upper images and θ' for the lower images.]

The formula used in the program for calculating the reflection coefficient from a lossy bottom is derived in the Appendix. The spatial phase term for each image is calculated from the distance. The pressure from an image is determined by multiplying the spatial phase factor with the total reflection coefficient and dividing it by the relevant distance. The summation of the complex pressure from every image is the complex pressure at the arbitrary receiver position.

In the pressure calculation for upper images, it is not necessary to calculate reflection coefficient for the first and second image. These two images don't interact with any bottom plane. The reflection coefficient for the first image is 1 and for the second is -1.

The resulting complex pressure from the upper family of images is

$$P_u = \sum_{n=1}^N \frac{1}{R(n)} \exp(-jkR(n)) \cdot (-1)^{\lfloor n/2 \rfloor} \prod_{m=1}^M R(\theta_{nm}) \quad (5.1)$$

$$\prod R(\theta_{nm}) = 1, \text{ for } n = 1, 2$$

and from the lower images is

$$P_l = \sum_{n=1}^N \frac{1}{R'(n)} \exp(-jkR'(n)) \cdot (-1)^{\lfloor n/2 \rfloor} \prod_{m=0}^M R(\theta'_{nm}) \quad (5.2)$$

In these expressions n indicates each image, and N is defined in Eqn. (1). The index m indicates each bottom and the number M is the total number of the bottom planes the sound meets during propagation to the receiver. It can be seen that

$$M = \lfloor (n-1)/2 \rfloor \quad (6)$$

The total complex pressure distribution P is the sum of the P_u and P_l :

$$P = P_u + P_l \quad (7)$$

R. PE MODEL

As stated above, two parabolic equation (PE) models were compared with the image method. The first was the PESAC model from Jensen and Tindle (1987) which is based on the wide-angle parabolic equation. The pressure field in the model has cylindrical symmetry about a vertical axis through the source position. The sloping bottom therefor forms a conical hill for downslope propagation and a conical bowl for upslope propagation. A line source was used for the majority of cases. In one downslope case they used a simple, standard Gaussian PE source, with a -3 dB half-width of 35° , a wedge angle of 10° and a frequency of 5 Hz. The contour graph for this case will be compared to the results of the image method and a second PE model.

The other PE model, PEIFD, was drawn from the thesis of Jaeger. This uses the implicit finite-difference (IFD) equation solution method to solve the PE. This method is unconditionally stable and has the capability to incorporate horizontal or sloping interfaces. The Fortran program in this thesis, like the PESAC model, specifies the receiver position with range and depth rather than range and angle. The input data used in this Fortran program were the same as the input data for Jensen and Tindle.

III COMPUTATION OF IMAGE METHOD

For the environmental parameters, the water has density ρ_1 and sound speed c_1 and the bottom has density ρ_2 , sound speed c_2 , and attenuation α/k_2 .

To verify spherical spreading close to the point source, source and receiver were positioned as in Fig. 6. With the receiver in the same angular plane as the source, the receiver range from the source was varied. The results, Fig. 7, verify that the pressure near the receiver has a $1/r$ dependence. In Fig. 7(a), the source is at a scaled distance $R_1 = 2$ and the multiplication of the range and the pressure is close to 1, as it should be. The relation between scaled and real distance will be illustrated in chapter 4 with a specific case. The very first point at unit range is inaccurate because of calculational round off.

Figure 7(b), where the source is at the scaled distance of $R_1 = 40$, shows the same dependence within calculational inaccuracy. In this graph there were no results at receiver ranges of 1, 2, 3 m because of data overflow when source is this close to the receiver. This overflow is due to the value of the $R(n)$. From Eqn. (3.1), $R(1)$, the distance from the first image to receiver (direct path), is very close to zero. This near zero condition is a denominator for the pressure calculation of Eqn. (5), thus causing an overflow.

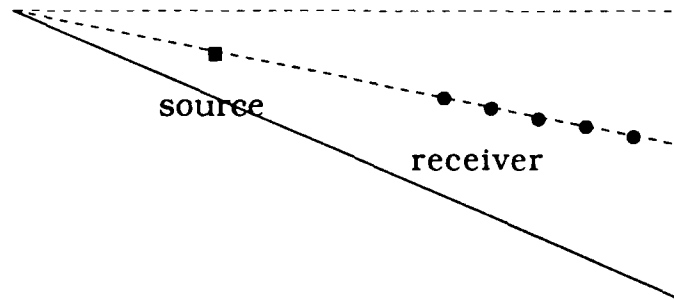
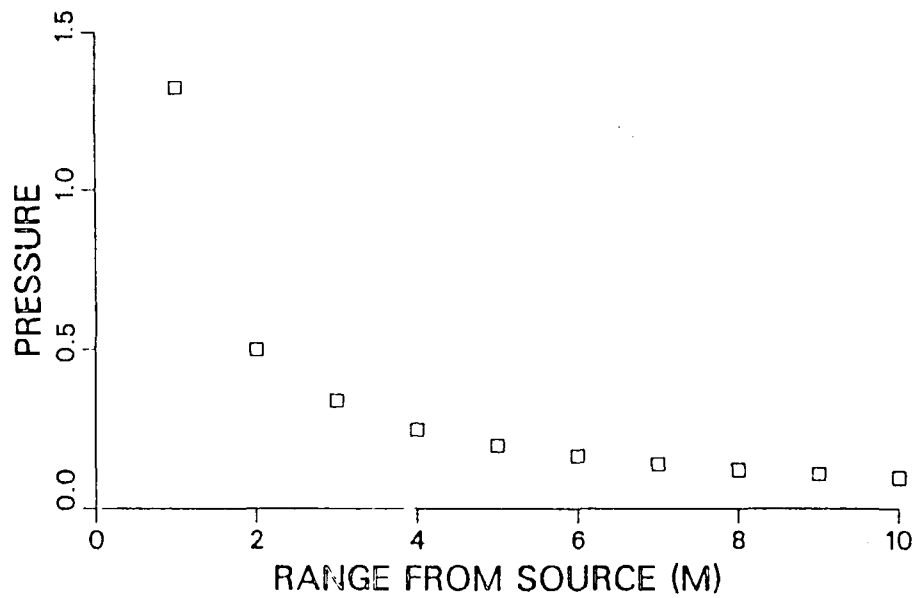
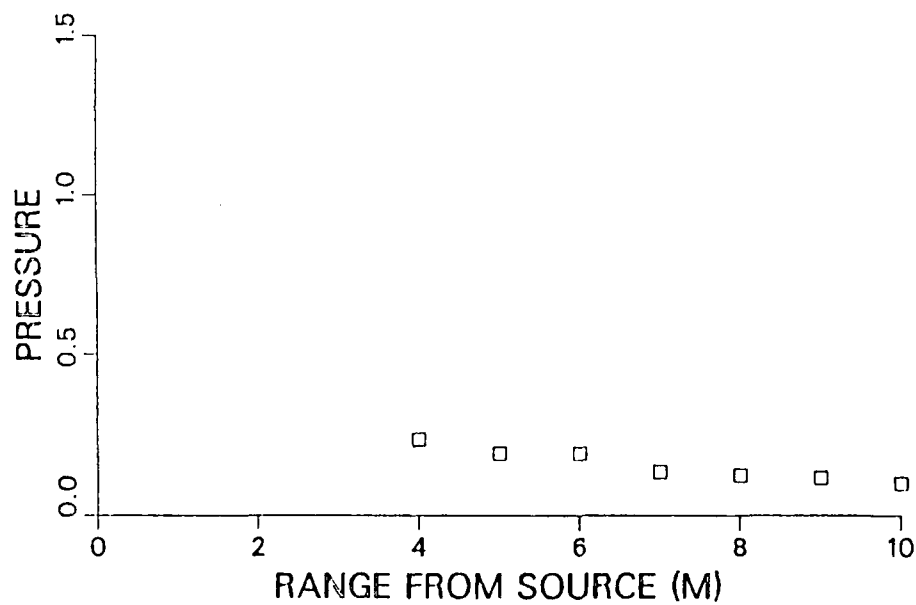


Figure 6. The positioning of the source and the receiver

The next three figures show dB loss vs position. For Fig. 8, the source is close to the apex and the pressure field is relatively simple, corresponding to the excitation of mostly the lowest mode. When the source range is relatively small this mode will dominate. The contour plots in Fig. 9 and 10 show that placing the source further from the apex excites the second mode. Placing the source even further from the apex will result in higher and more complex modes being excited. All the distances in Fig. 8, 9 and 10 are scaled distances. It is easy to show that the nondimensional cutoff distances of the first few modes are approximately 3, 5, 7, 11,



(a) source distance $R_1 = 2$



(b) source distance $R_1 = 40$

Figure 7. The range $R(1)$ dependence of the pressure in the image method. Frequency 5 Hz, $D_1 = 0.5$, $CC = 5/6$, $\beta = 10^\circ$, $\gamma = \delta = 5^\circ$

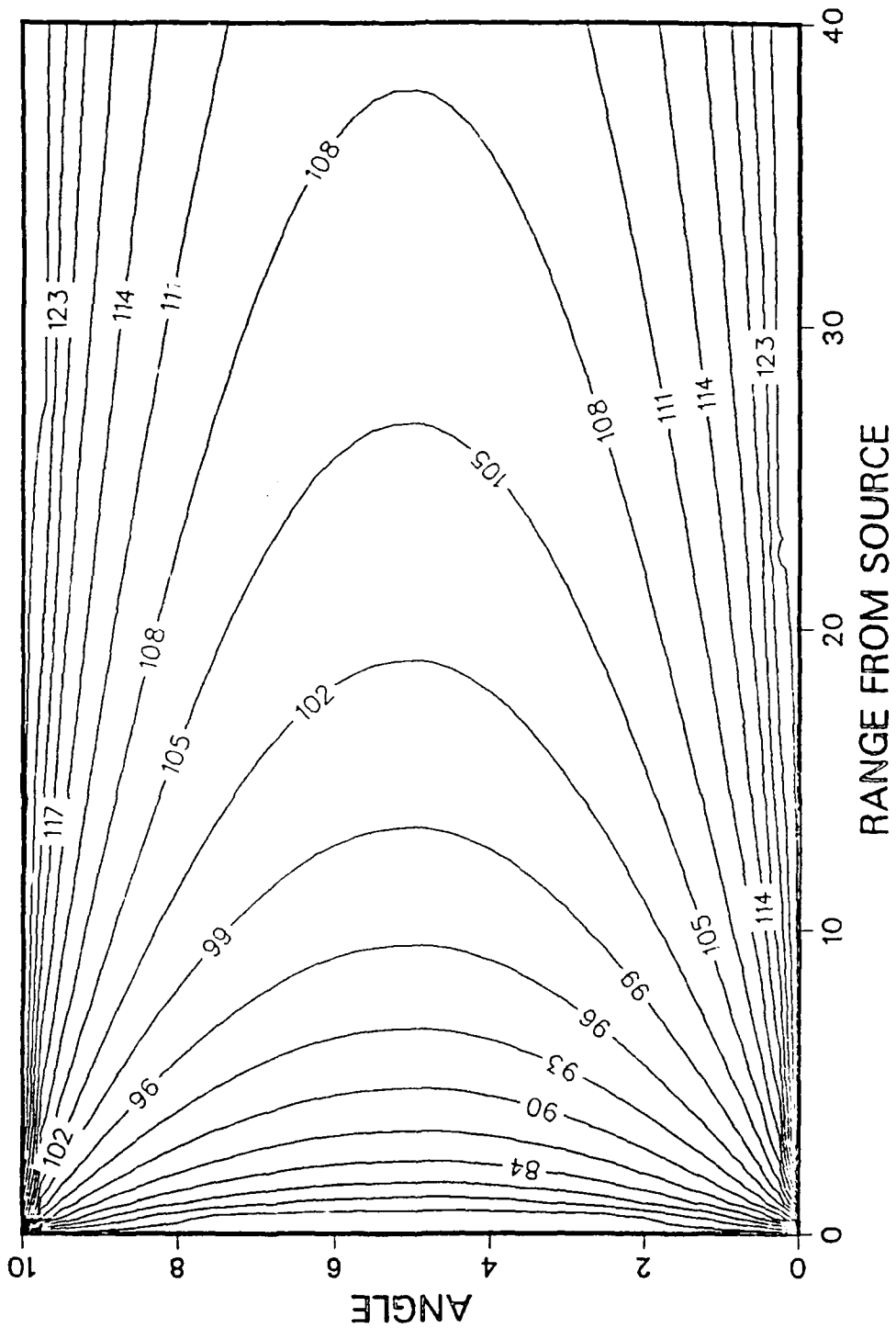


Figure 8. Excitation of mode 1, $\beta = 10^\circ$, $R_1 = 2$ and the rest of parameters same as in Fig. 7

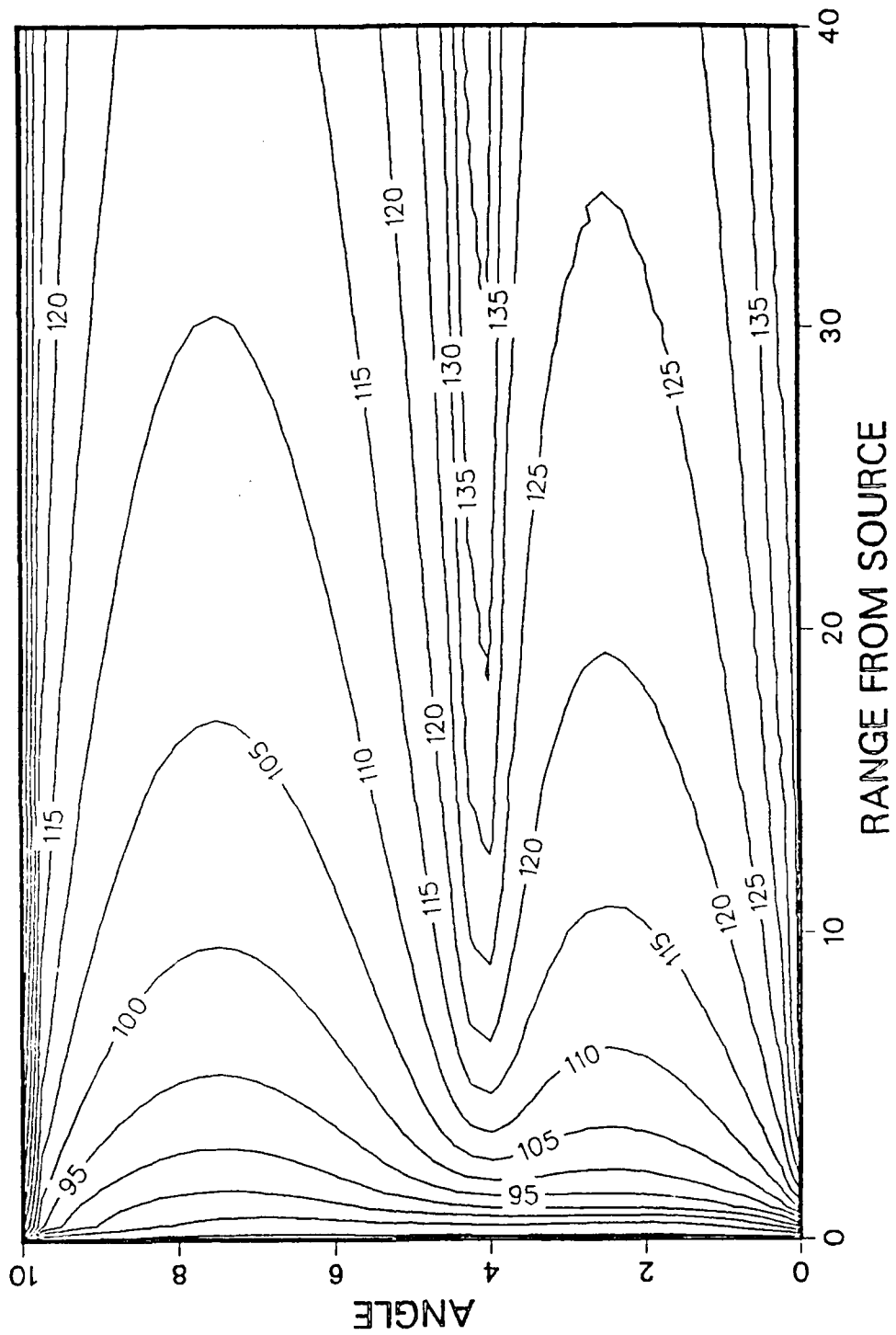


Figure 9. Mode 2 in a wedge, $R_1 = 4.5$, the rest of parameters same as Fig. 7

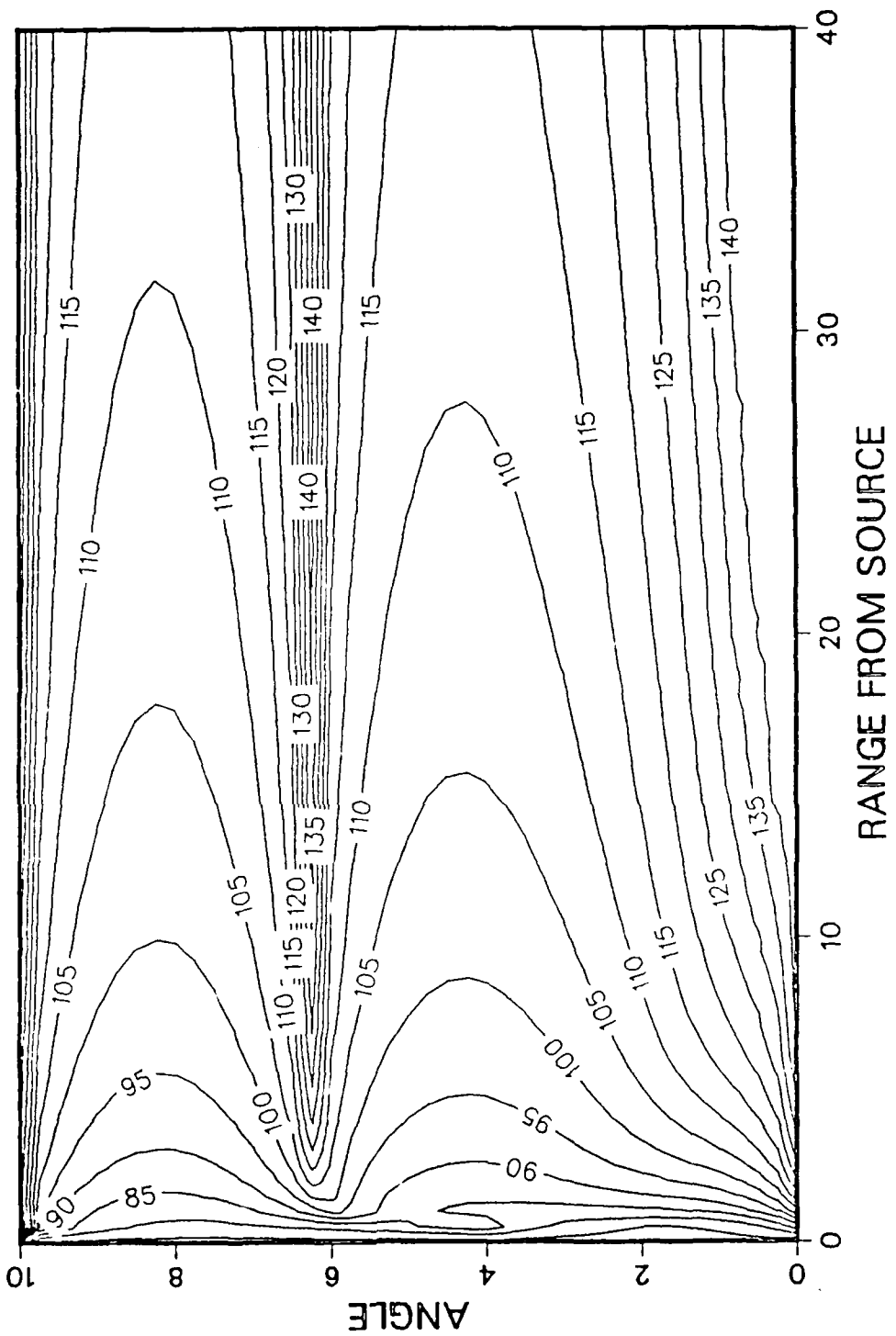


Figure 10. Mode 2 in a wedge, $R_1 = 6$, the rest of parameters same as Fig. 7

IV. DISCUSSION

A. IMAGE METHOD AND PESAC

The contour plot from Jensen and Tindle (1987) is shown in Fig. 12(a). The input data for this contour are given by Table 1. The input data for the image method was chosen to be the same.

The contour lines in Fig 12(a), which indicate dB loss, show that propagation is almost entirely in mode 1. In this figure, the frequency was 5.0 Hz, source depth (SD) was 50 m, water depth was 100 m and the maximum range was 10 km.

To compare this with the image method, geometric parameters from the PE model were translated to parameters for the image method using Fig. 11. Source distance R_1 , source angle γ , and horizontal distance x for image method can be found from the wedge angle, water depth and source depth of the PE model. From simple geometric calculation, $x = 567.13$ m, $\gamma = 4.96^\circ$, $R_1 = 569.33$ m.

TABLE 1. PARAMETERS FOR MEDIA USED BY JENSEN AND TINDLE (1987)

	density($17 \cdot m^{-1}$)	sound speed	attenuation
water	$\rho_1 = 1000$	$c_1 = 1500$ m/s	
bottom	$\rho_2 = 2000$	$c_2 = 1800$	$a\lambda_2 = 1$ dB

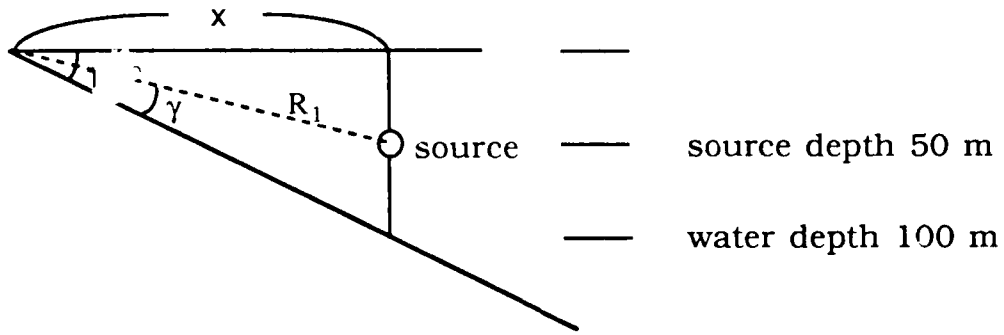


Figure 11. Conversion of source distance and angle for image method from Jensen and Tindle (1987)

To input ranges into the image method program, they should be converted to a scaled range. To convert R_1 and R_2 into the scaled range, the following formula is applied.

$$k_1 X = \frac{\pi}{2 \sin \theta_c \tan \beta}$$

where X is the scaling range

This scaled range is used in the image method program. The relation between scaled range and real range is

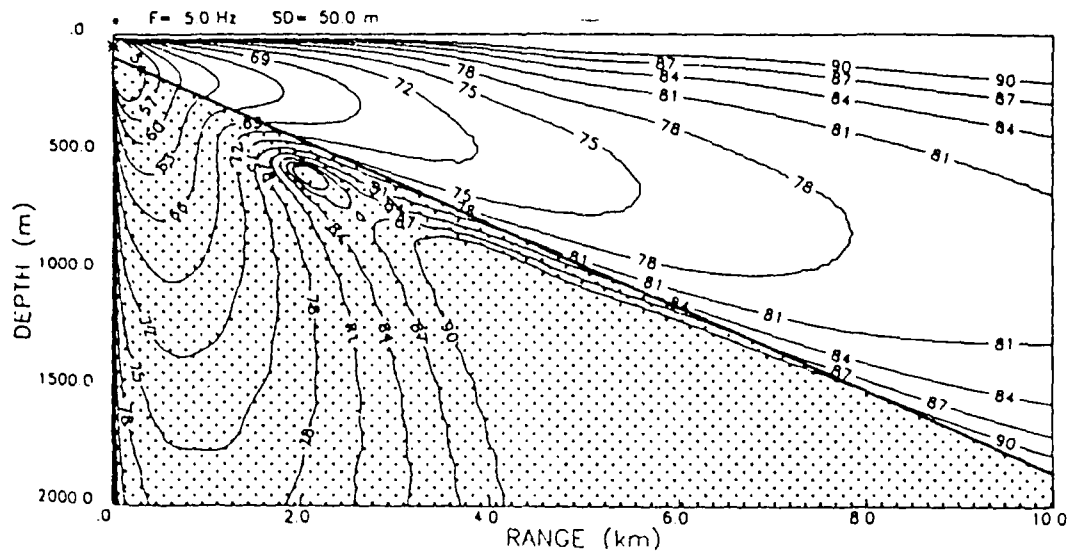
$$R(\text{scaled range}) = R(\text{real}) / X$$

The critical angle (θ_c) is calculated to be 33.56° . With this critical angle, a wedge angle of 10° , and a frequency of 5.0 Hz, $X = 769.48$ m. This gives a scaled distance for R_1 of 0.74. A scaled distance of $R_2 = 13.2$ corresponds to the map range of 10.154 km. (The distance R_2 is measured from source to the receiver directly in the image method but horizontally in the PE model.)

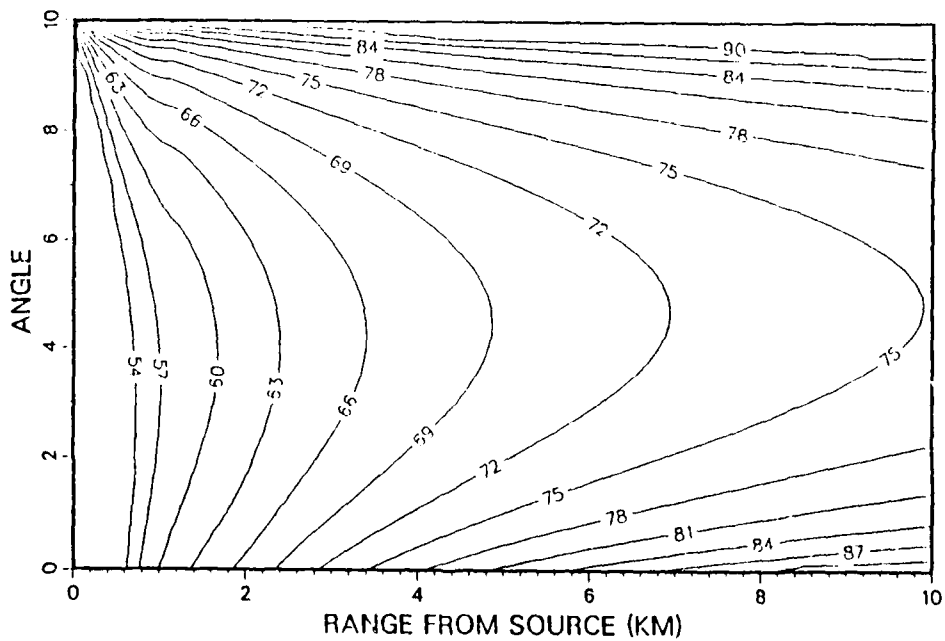
The attenuation in the PE model of $a\lambda_2 = 1$ dB is equivalent to $\alpha/k_2 = 0.0183$ for the image method since

$$\alpha/k_2 = a\lambda_2/(8.7 \times 2 \pi)$$

The transmission loss contours from the image method are shown in Fig. 12(b). These two contours show very similar shape. Figure 13 is an overplot of image-method results on the contour plot of the PE model. Near the surface and in the mid-depth level, the image method has 3 to 5 dB less loss, while they agree well near the bottom.



(a)



(b)

Figure 12. Contour plots (a) Jensen and Tindle, (b) Image method

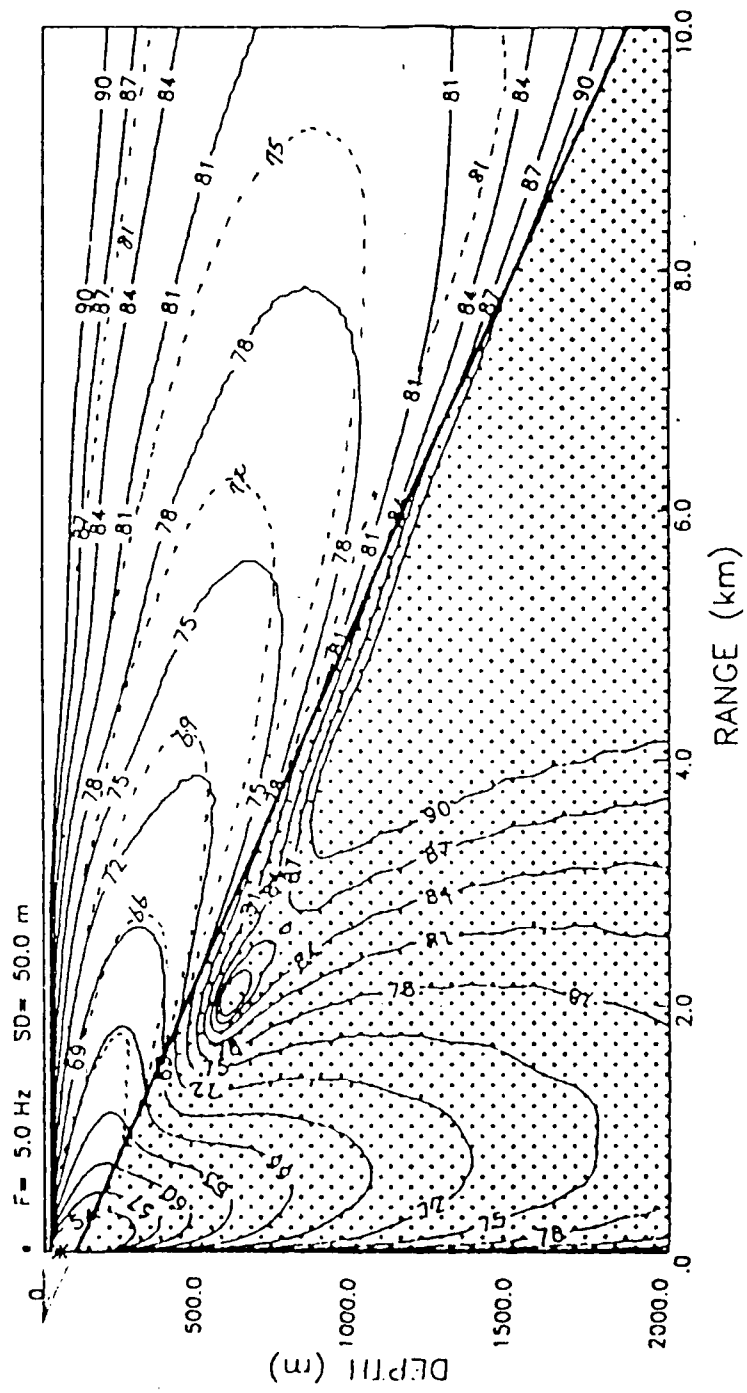


Figure 13. Overplot of Fig. 11 and 12

B. IMAGE METHOD AND PEIFD

The PEIFD model is designed to generate transmission loss both in the bottom and in the water along horizontal range from the source at a given depth. The image method program was run in such a manner as to yield comparisons between the image method and this PE model.

The input file used for this purpose is shown in Table 2. The number in column 1, row 1 is the frequency in Hz and column 3, row 1 is the receiver depth in m which was varied to probe the entire sound field, both in the water and in the bottom. Rows 3 and 4 define the sloping bottom and the definition of the remaining terms can be found in Ref. 2.

In the image method, to find the pressure as a function of horizontal range at constant depth, the receiver angle must be changed, as the range is changed, as shown in Fig. 14.

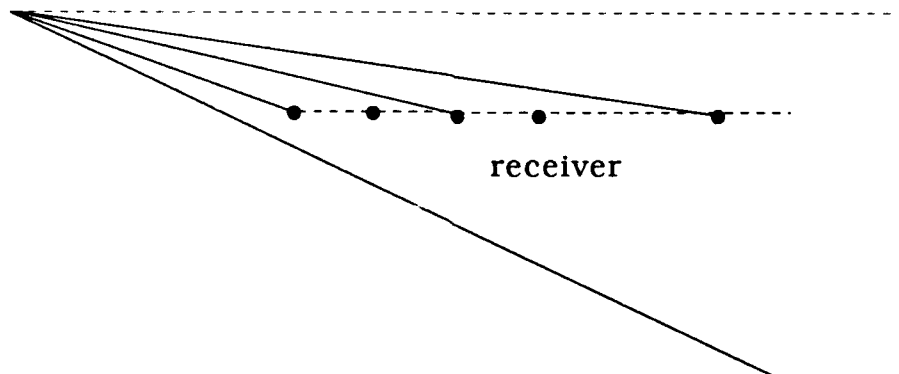


Figure 14. Receiver along horizontal range

TABLE 2. INPUT DATA FILE FOR THE PE

<u>5</u>	50	<u>500</u>	0	4000	
10000	0.0	0.0	50	1000	25
<u>0</u>	<u>100</u>				
<u>10000</u>	<u>1763</u>				
-1	-1				
1763	1.0	0.0			
0	1500				
1000	1500				
1763	1500				
8000	2.0	1.0	1800		
6000					

The graphs shown in Fig. 15 through 22 indicate the results of the PEIFD model with a solid line and the image method with a dashed line. The PESAC model is annotated with the 'o' connected by dashes for selected graphs. The graphs are dB loss versus horizontal range in km at a fixed depth and all the source and receiver parameters are the same as used in the Jensen and Tindle model. The difference between the image method and PEIFD is approximately 2 to 3 dB in shallow water and the two lines converge as depth increases. The PEIFD results in the bottom also have a similar shape to the PESAC results.

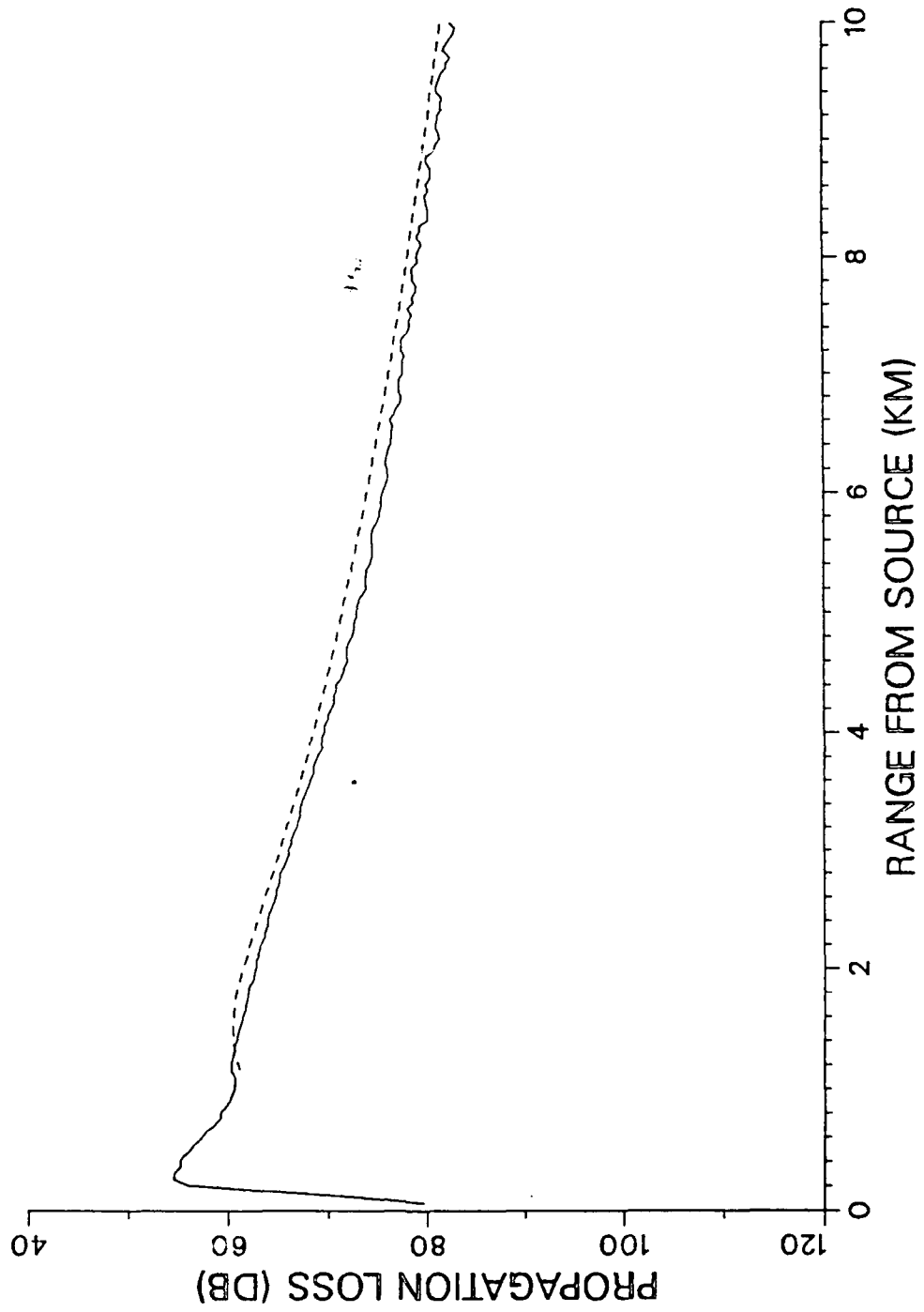


Figure 15. dB loss .vs. range, depth = 50 m

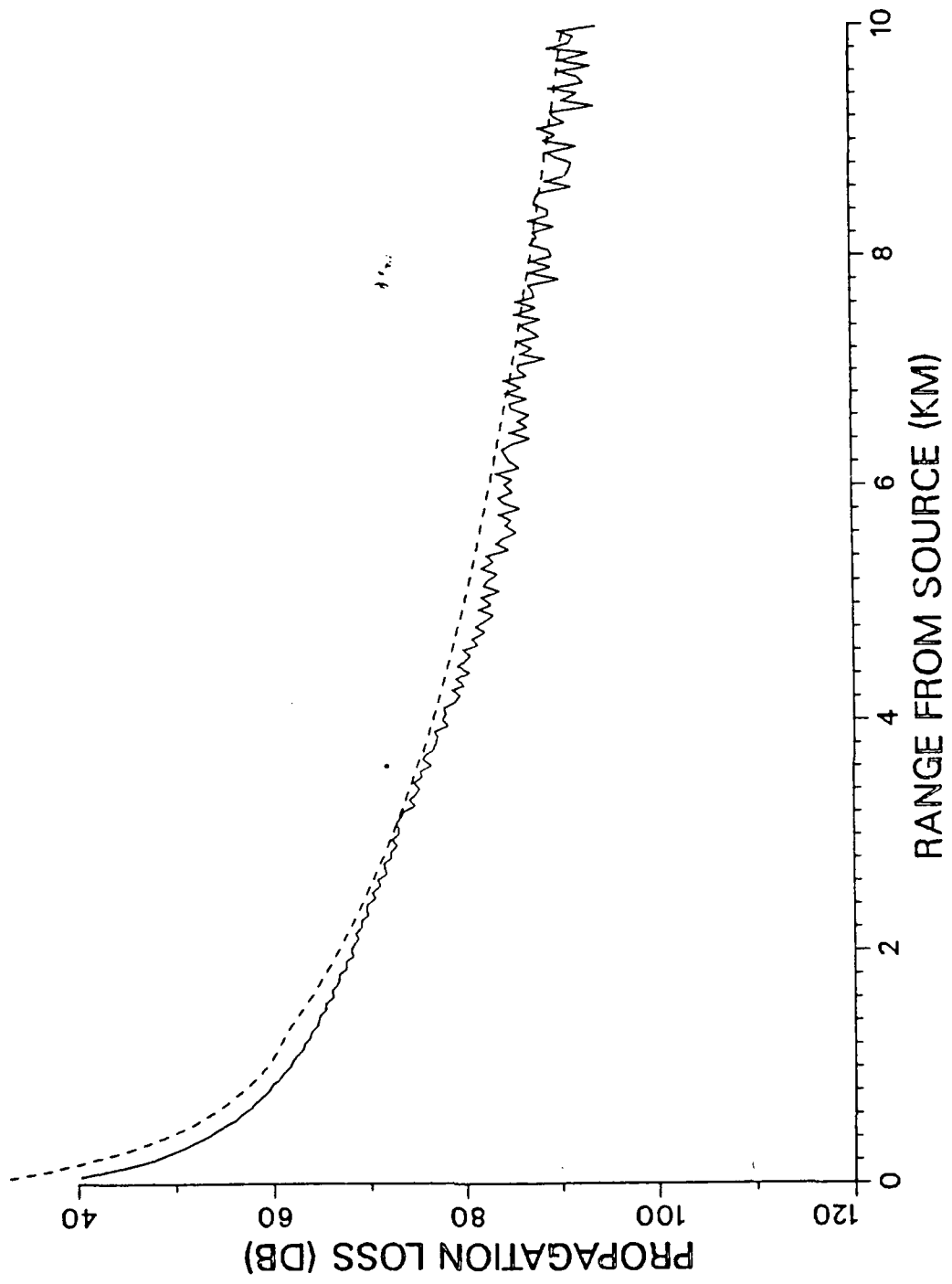


Figure 16. dB loss .vs. range, depth = 100 m

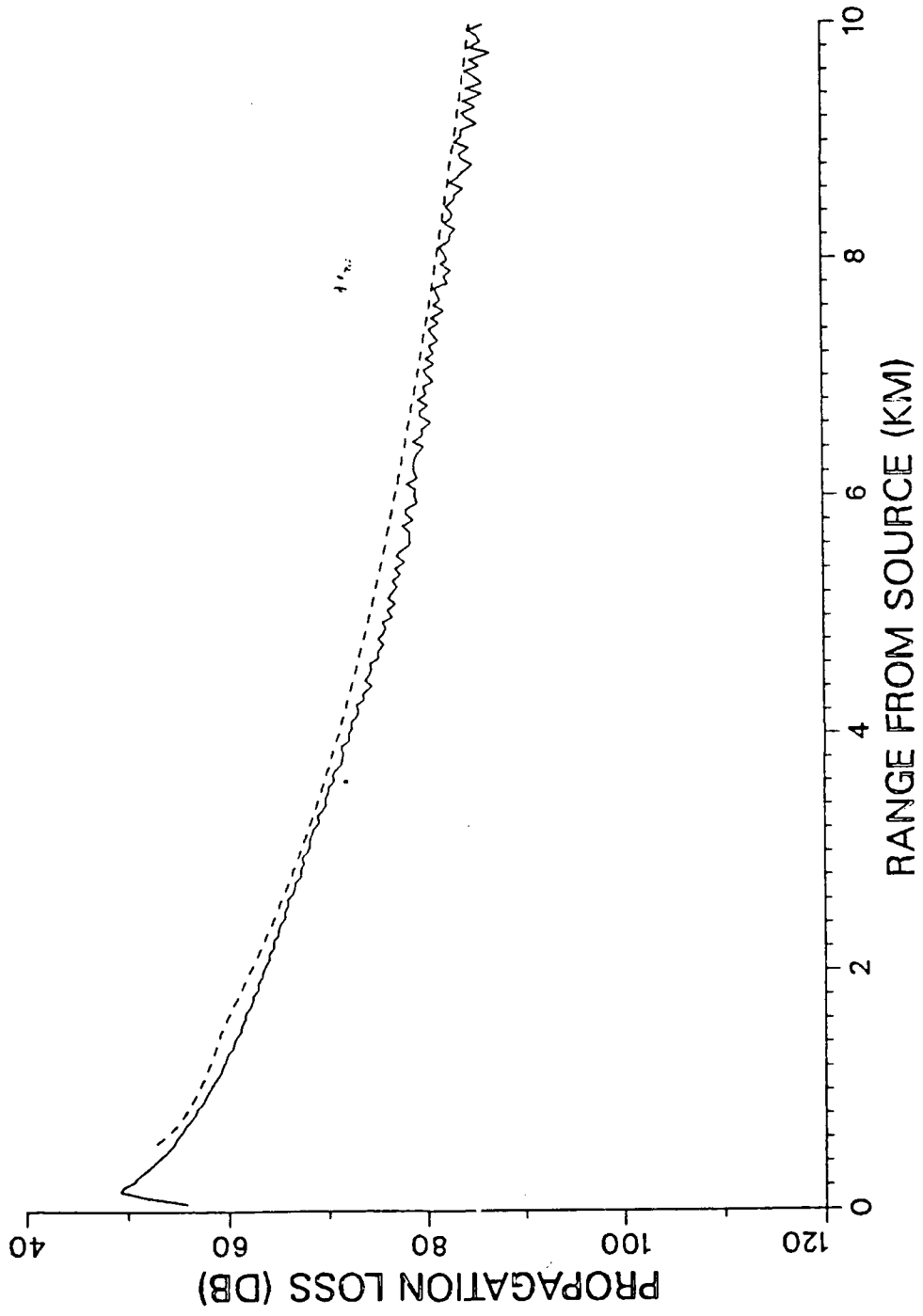


Figure 17. dB loss .vs. range, depth = 200 m

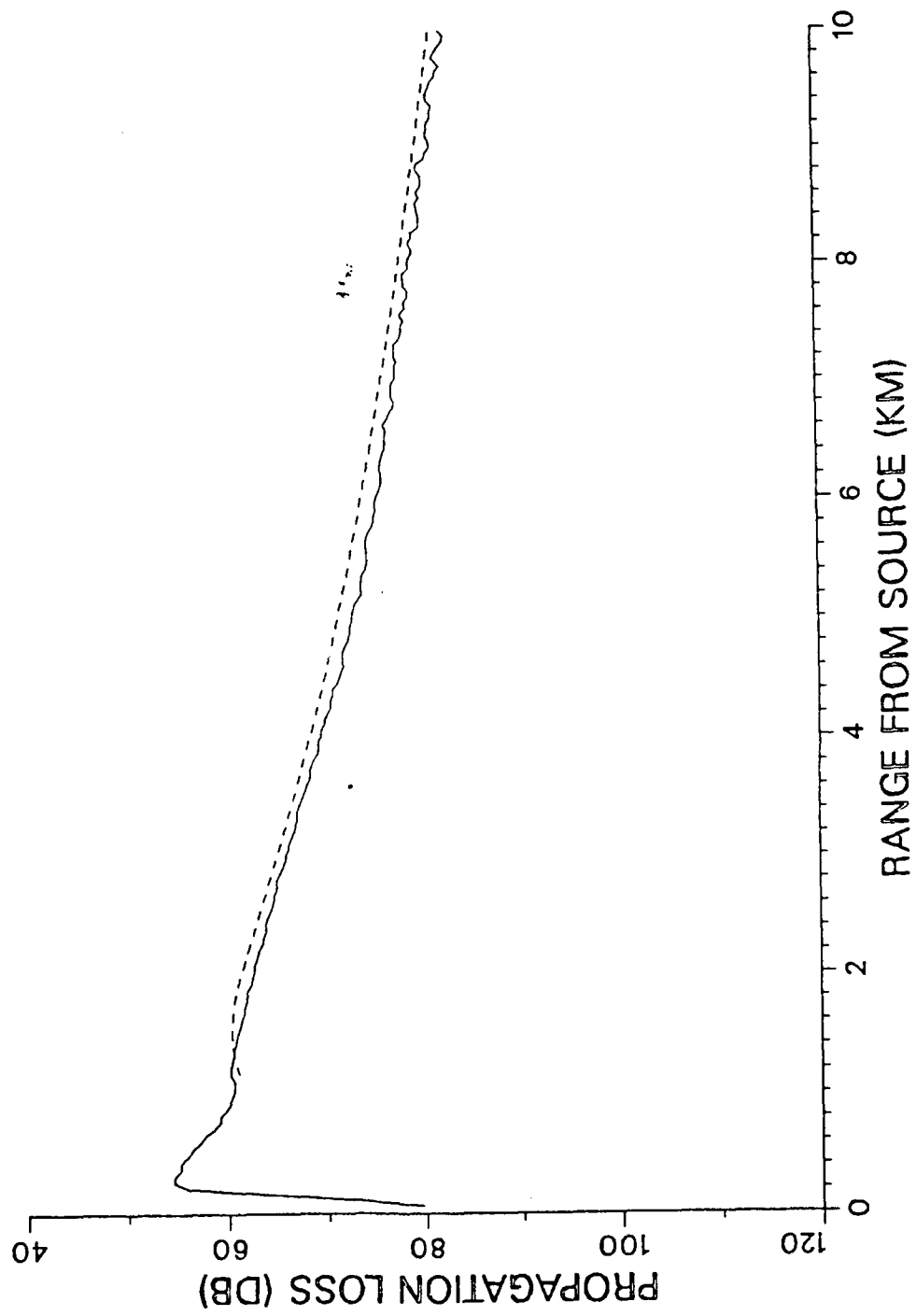


Figure 18. dB loss .vs. range, depth = 300 m

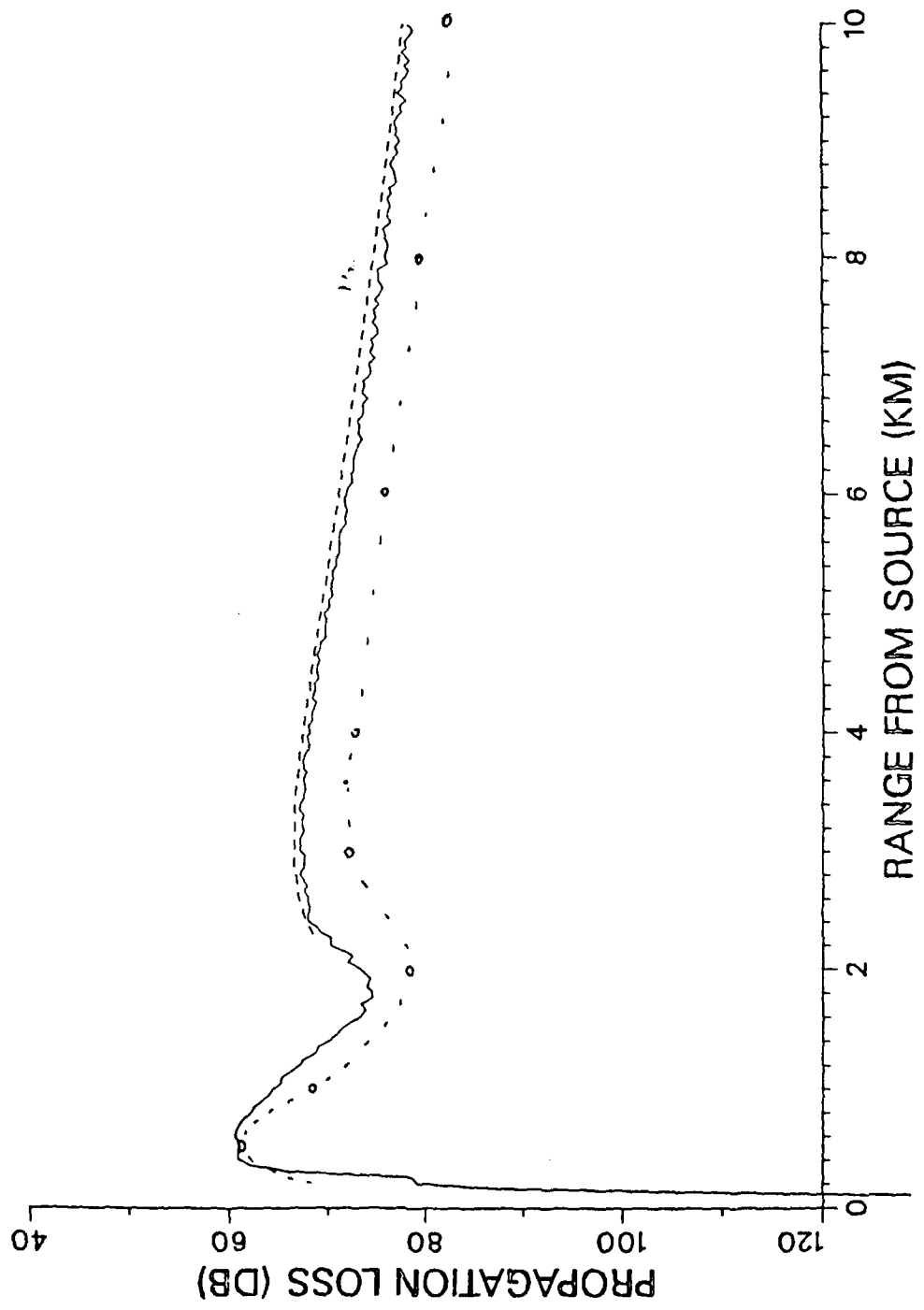


Figure 19. dB loss vs. range, depth = 500 m

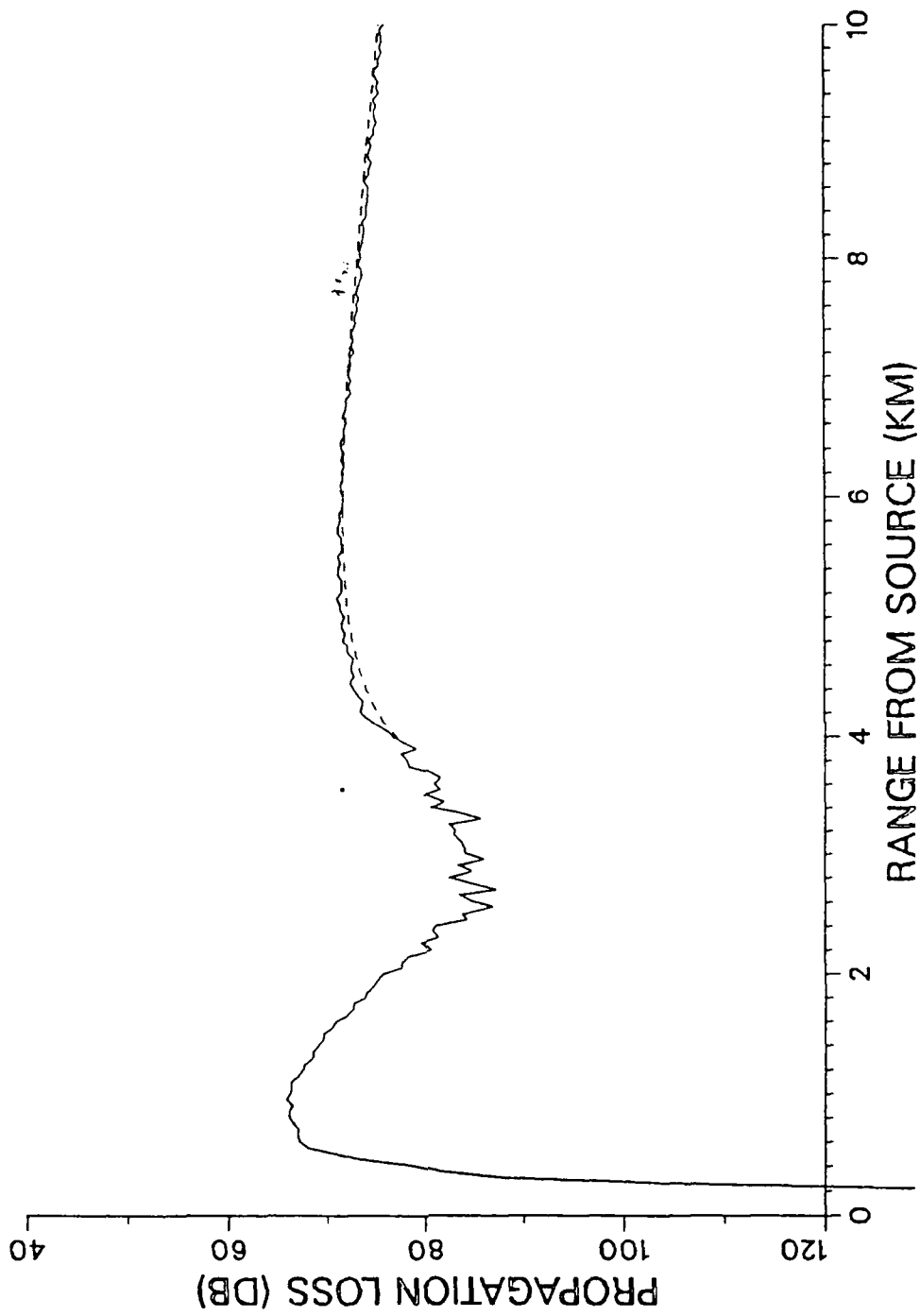


Figure 20. dB loss .vs. range, depth = 800 m

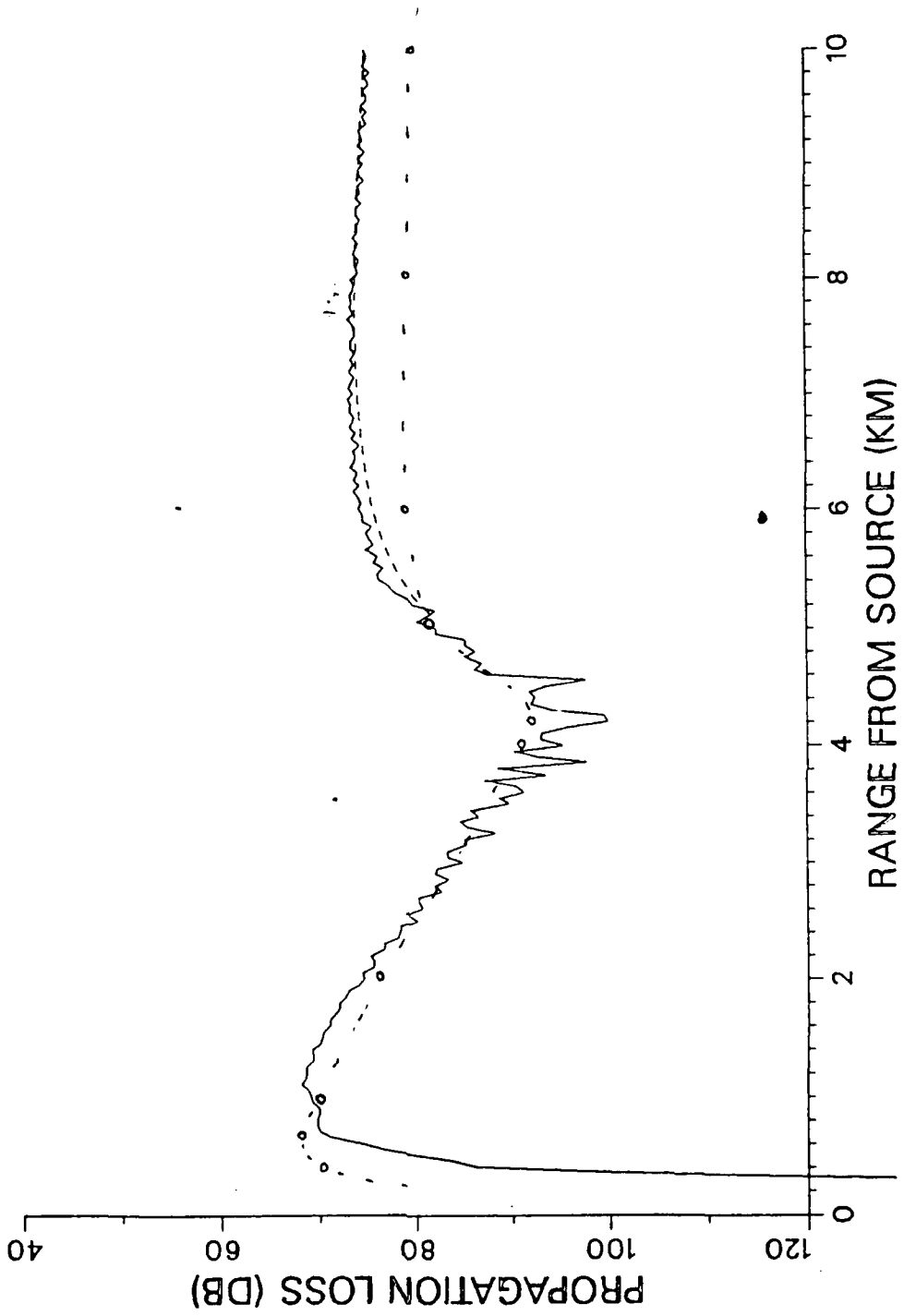


Figure 21. dB loss .vs. range, depth = 1000 m

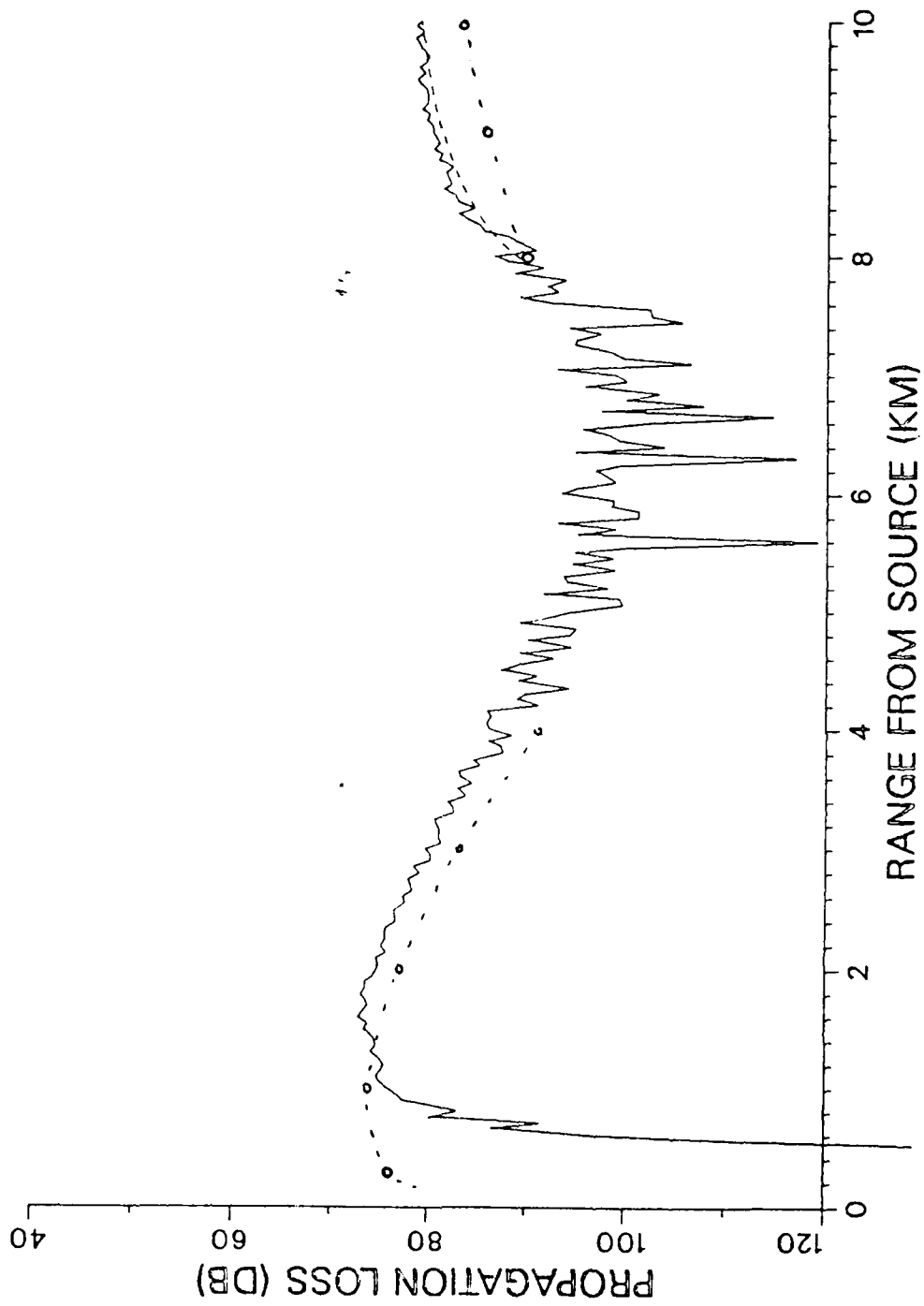


Figure 22. dB loss .vs. range, depth = 1500 m

V. CONCLUSIONS

The geometric implementation of the ocean wedge and its boundaries by the image method and the PE models are different. To validate the use of these very different geometric models it is important to know how well they agree with each other for specific geometries. This thesis was an attempt to compare the image method and two PE models for propagation direction down slope and with only one mode excited.

Between the contour plot of the image method and PESAC model, there is a 3 to 5 dB difference at mid-depths. This difference may be due to different normalization techniques or to the basic difference in geometry, but this hypothesis cannot be verified because the PESAC program was not available. The plot, however, shows a very similar shape for the two models.

On the other hand, when the image method is compared with the PEIFD model, the results show good agreement overall, with slightly less agreement at shallow depths. This would suggest that the different geometry may not lead to different TL's in this range of comparisons. Overall, however, since the image method compares quite favorably with both PE models, all three are apparently good tools for underwater sound prediction for downslope propagation with only one mode propagating. It is still an unresolved question how the various models will compare for upslope propagation, cross-slope propagation, and the source positioned to excite more than one mode.

APPENDIX

The reflection coefficient is given by

$$V = \frac{\frac{\rho_2}{\rho_1} \sin \theta - \frac{c_1}{c_2} \sin \theta_t}{\frac{\rho_2}{\rho_1} \sin \theta + \frac{c_1}{c_2} \sin \theta_t}$$

where θ is incident angle

θ_t is transmission angle

subscript 1 denotes water and 2 bottom

and

$$\sin \theta_t = \sqrt{1 - (c_2 / c_1)^2 \cos^2 \theta}$$

then

$$\frac{c_1}{c_2} \sin \theta_t = \sqrt{(c_1 / c_2)^2 - \cos^2 \theta}$$

With lossy bottom

$$\frac{c_1}{\bar{c}_2} = \frac{c_1}{c_2(1 - j\alpha / k_2)} \cong \frac{c_1}{c_2}(1 + j\alpha / k_2)$$

and

$$\left(\frac{c_1}{\bar{c}_2}\right)^2 = (c_1 / c_2)^2 (1 + j\alpha / k_2)^2 \cong (c_1 / c_2)^2 + 2j(c_1 / c_2)^2 \alpha / k_2$$

makes

$$\frac{c_1}{\bar{c}_2} \sin \theta_t = \sqrt{(c_1 / c_2)^2 - \cos^2 \theta + 2j(c_1 / c_2)^2 \alpha / k_2}$$

Let

$$\frac{c_1}{\bar{c}_2} \sin \theta_t = \sqrt{a - jb} = (a^2 + b^2)^{1/4} e^{j\phi/2}$$

where

$$a = (c_1 / c_2)^2 - \cos^2 \theta, \quad b = 2(c_1 / c_2)^2 \alpha / k_2, \quad \phi = \tan^{-1} \frac{b}{a}$$

With trigonometric identity

$$\begin{aligned} e^{j\phi/2} &= \sqrt{\frac{1 + \sqrt{1 + (b/a)^2}}{2\sqrt{1 + (b/a)^2}}} - j \sqrt{\frac{\sqrt{1 + (b/a)^2} - 1}{2\sqrt{1 + (b/a)^2}}} \\ &= \sqrt{\frac{\sqrt{b^2 + a^2} + a}{2\sqrt{b^2 + a^2}}} - j \sqrt{\frac{\sqrt{b^2 + a^2} - a}{2\sqrt{b^2 + a^2}}} \end{aligned}$$

Utilizing this

$$\begin{aligned} \sqrt{2} \frac{c_1}{\bar{c}_2} \sin \theta_t &= \sqrt{\sqrt{b^2 + a^2} + a} - j \sqrt{\sqrt{b^2 + a^2} - a} \\ V &= \frac{\frac{\rho_2}{\rho_1} \sin \theta - \frac{1}{\sqrt{2}} \sqrt{\sqrt{b^2 + a^2} + a} + j \frac{1}{\sqrt{2}} \sqrt{\sqrt{b^2 + a^2} - a}}{\frac{\rho_2}{\rho_1} \sin \theta + \frac{1}{\sqrt{2}} \sqrt{\sqrt{b^2 + a^2} + a} - j \frac{1}{\sqrt{2}} \sqrt{\sqrt{b^2 + a^2} - a}} \end{aligned}$$

This form of the reflection coefficient is used to find pressure field in the program code for the image method.

LIST OF REFERENCES

1. Jensen, F. B., and Tindle, C. T., "Numerical Modeling Results for Mode Propagation in a Wedge," *J.A.S.A.*, v. 82(1), pp. 211-216, July 1987.
2. Jaeger, L. E., *A Computer Program for Solving the Parabolic Equation Using an Implicit Finite-Difference Solution Method Incorporating Exact Interface Conditions*, Master's Thesis, Naval Postgraduate School, Monterey, California, September 1983.
3. Naval Postgraduate School Report 61-79-002, *Programs for the Evaluation of the Acoustic Pressure Amplitude and Phase at the Bottom of a Wedge-Shaped Fluid Layer Overlaying a Fast Fluid Half Space*, by Coppens, A. B., Sanders, J. V., Ioannou, I., and Kawamura, W., December 1978.
4. Baek, C. K., *The Acoustic Pressure in a Wedge-Shaped Water Layer Overlying a Fast Fluid Bottom*, Master's Thesis, Naval Postgraduate School, Monterey, California, March 1984.
5. LeSesne, P. K., *Development of Computer Programs Using the Method of Images to Predict the Sound Field in a Wedge Overlying a Fast Fluid and Comparison with Laboratory Experiments*, Master's Thesis, Naval Postgraduate School, Monterey, California, December 1984.

INITIAL DISTRIBUTION LIST

	No. Copies
1. Defense Technical Information Center Cameron Station Alexandria, VA 22304-6145	2
2. Library Code 52 Naval Postgraduate School Monterey, CA 93943-5002	2
3. Dr. K. E. Woehler, Code PH/Wh Chairman, Department of Physics Naval Postgraduate School Monterey, California 93943-5002	1
4. Dr. A. B. Coppens, Code PH/Cz Department of Physics and Chemistry Naval Postgraduate School Monterey, California 93943-5002	2
5. Dr. J. V. Sanders, Code PH/Sd Department of Physics and Chemistry Naval Postgraduate School Monterey, California 93943-5002	2
6. Dr. Ching-Sang Chiu, Code OC/Ci Department of Oceanography Naval Postgraduate School Monterey, California 93943-5002	1
7. Dr. T. G. Muir Univ. of Texas, Applied Research Labs., P.O. Box 8029 Austin, Tx 78713-8029	1

8. Dr. Robert H. Bourke, Code OC/Bf 1
Department of Oceanography
Naval Postgraduate School
Monterey, California 93943-5002

9. Dr. F. B. Jensen 1
SACLANT Undersea Research Ctr., 090195000 APO
New York, NY 39-187-540111

10. Dr. Sehung Kwak, Code CS/Kw 1
Department of Computer Science
Naval Postgraduate School
Monterey, California 93943-5002

11. Lt. Kim, Jong Rok 4
Lucky APT. 18 Dong 207 Ho
707, OnCheon 2 Dong, DongRae Gu
Pusan, Korea

12. Yoon, Hye Byung 1
S.M.C. 2137, Naval Postgraduate School
Monterey, California 93943